Water Management

Model of flow over spillways by computational fluid dynamics
Chinnarasri, Kositgittiwong and Julien

ice | proceedings

Proceedings of the Institution of Civil Engineers

http://dx.doi.org/10.1680/wama.12.00034
Paper 1200034
Received 26/01/2012 Accepted 05/07/2012
Keywords: Keywords: hydraulics & hydrodynamics/mathematical modelling/ models (physical)

ice Institution of Civil Engineers publishing

Model of flow over spillways by computational fluid dynamics

1 Chaiyuth Chinnarasri PhD
Professor, Water Resources Engineering & Management Research Center (WAREE), King Mongkut's University of Technology Thonburi, Bangkok, Thailand

2 Duangrudee Kositgittiwong BEng
PhD Candidate, Water Resources Engineering & Management Research Center (WAREE), King Mongkut's University of Technology Thonburi, Bangkok, Thailand

3 Pierre Y. Julien PhD
Professor, Department of Civil and Environmental Engineering, Colorado State University, USA



The objective of the present study was to simulate the flow behaviour through smooth, 25-step and 50-step spillways using a multiphase flow model with the realisable k–ε model. The simulation results were compared with the data from a large-scale physical model. A grid convergence index was used to reduce the discretisation error. The simulation results of flow along stepped spillways and the flow on the step agreed well with experimental data for both smooth and stepped spillways. The flow profiles, velocity profiles, turbulence intensity, and energy dissipation of flow through spillways are illustrated and discussed. Expressions for the turbulence intensity distributions in smooth and stepped spillways are also proposed.

NOTATION

C_1	$\max[0{\cdot}43, \eta/(\eta+5)]$, $\eta = Sk/\varepsilon$
C_2	constant of 1·9
$C_{1\varepsilon}$	constant of 1·44
$C_{3\varepsilon}$	relation of flow velocity in x and y-direction, $C_{3\varepsilon} = \tanh\lvert v/u\rvert$
D	constants of distribution of turbulence intensity
e_a^{ij}	approximate relative error (%)
e_{ext}^{ij}	extrapolated relative error (%)
E_0	energy at the inlet section, $E_0 =$ (elevation head + $1{\cdot}5y_c$) (m)
E_i	energy at the point-of-interest section, $E_i =$ (flow depth measured in vertical direction + velocity head) (m)
E_L	energy loss $E_L = E_0 - E_i$ (m)
f	value of numerical solution $f_{ij} = f_i - f_j$
f_{ext}^{ij}	extrapolated numerical solution
F_s	safety factor
G_b	generation of k due to buoyancy kg/(ms^3)
G_k	generation of k due to the fluid shear, $G_k = \mu_t S^2$ kg/(ms^3)
h	step height (m)
H	flow depth normal to the slope (m)
i	index of step number
I	turbulence intensity, $I = u'/V$
k	turbulent kinetic energy (m^2/s^2)
K_s	roughness height, $K_s = h\cos\theta$ (m)
l	step length (m)
L	spillway length in streamwise direction from upstream of spillway (m)
L_S	length in streamwise direction from upstream of spillway to the point of interest (m)
n	exponent number of power law
N	total number of steps along the spillway
N_t	total number of cells
P	pressure (N/m^2)
p	apparent order for Grid Convergence Index
r_{ij}	grid refinement ratio, $r_{ij} = h_{gi}/h_{gj}$, i and j are mean coarse and fine grids, respectively
Re	Reynolds number
s	relative horizontal distance $s = il/L\cos\theta$
S	modulus of the mean rate of strain tensor, $S = \sqrt{2S_{ij}S_{ij}}$ (1/s)
S_k	source terms of kinetic energy kg/(ms^3)
S_ε	source terms of dissipation rate kg/(ms^4)
t	time (s)
u_i	velocity in x_i-direction (m/s)
u_j	velocity in x_j –direction (m/s)
u_*	friction velocity (m/s)
u'	fluctuating velocity (m/s)
V	velocity at point of interest (m/s)
V_{90}	velocity at the depth of 90% air concentration (m/s)
y	depth at point of interest normal to the slope (m)

y_c critical depth (m)
Y_M effect of compressibility on turbulence kg/(ms^3)
α_a volume fraction of air (%)
α_w volume fraction of water (%)
ε turbulent dissipation rate (m^2/s^3)
λ exponent number of distribution of turbulence intensity
μ molecular dynamic viscosity kg/(ms)
μ_t turbulent dynamic viscosity kg/(ms)
ν kinematic viscosity (m^2/s)
θ spillway slope (°)
ρ cell density (kg/m^3)
ρ_a air density (kg/m^3)
ρ_w water density (kg/m^3)
σ_k turbulent Prandtl number for k, $\sigma_k = 1{\cdot}0$
σ_ε turbulent Prandtl number for ε, $\sigma_\varepsilon = 1{\cdot}2$
ω turbulent frequency (l/s)

1. Introduction

A spillway is an important facility designed to prevent overtopping and release flood flow. Due to the high flow over the spillway the design is complicated and gives rise to cavitations and high kinetic energy problems. A stepped spillway having a profile made up of a number of steps and consisting of an open channel with a series of drops is becoming popular for high-efficiency controlled release of overflow. The step faces can dissipate the energy of the flow and reduce the size of the energy dissipator needed downstream of the spillway. The aerated flow on the stepped spillway also reduces cavitation problems (Chamani and Rajaratnam, 1999). Scaled-down models of spillways have been used as tools to study the flow over stepped spillways. Many studies have investigated various sizes of stepped spillways experimentally, but they were very expensive and time-consuming due to the complexity of the flow.

In highly air-entrained flows such as two-phase flow through a spillway, the viscous forces and surface tension play a very important role in air entrainment. If these two secondary forces are ignored a scale effect, a critical term of the problem which is used to describe slight distortions, can occur and the data can then be misinterpreted. The physical modelling of stepped spillways based upon a Froude similitude may be sensitive to scale effects (Gonzalez and Chanson, 2004). If a Froude similitude is applied, the air bubbles are too large and cause a detrainment rate that is too high. Moreover, flow recirculation on the step causes a momentum exchange with the main flow and suggests the need for a Reynolds similitude. A Reynolds number of at least 10^5 is proposed to minimise viscous effects (Boes and Hager, 2003). A scale of 10:1 or larger is suggested for reducing the scale effects in modelling stepped spillways (Chanson, 2002). A minimum Weber number of 100 is recommended for surface tension effects to be negligible (Boes and Hager, 2003; Gonzalez and Chanson, 2004).

As experiments are both expensive and time-consuming, the use of high-performance computers together with further developments in computational fluid dynamics (CFD) are important in order to investigate flow over spillways using reasonable resources, time and expense. Chen *et al.* (2002) used a standard k–ε model to simulate the flow. The first five step heights were 0·02, 0·024, 0·03, 0·04 and 0·05 m. Downstream were eight more steps with a uniform step height of 0·06 m. The overall height of the spillway was 0·789 m and the number of steps was only 13, yielding a model which was too short to attain the aerated zone. The trends of the velocity and pressure profiles from the numerical and physical models were similar but the error at some points was more than 20%. However, the results proved to be consistent with the flow characteristics and measured surface profiles. Cheng *et al.* (2006) used a mixture model to reproduce the flow over a stepped spillway, and also included the interaction between entrained air and cavity recirculation in the flow, velocity distribution and the pressure profiles on the step surface.

However, even if the numerical solution agrees well with experiment data, there is the uncertainty arising from discretisation errors. The discretisation error is a potential deficiency in any phase of the modelling process due to lack of knowledge. Therefore, a grid independence study has recently become an important tool to determine whether the grid size is refined enough to produce good results with less discretisation error.

The aim of the present study was to extend the understanding of the flow through spillways by using numerical results. Herein, a suggestion for appropriate grid size for the simulation is presented, based on the grid convergence index (GCI). The flow profiles, velocity profiles, turbulence intensity, and energy dissipation are illustrated and discussed. Finally, expressions for the turbulence intensity distributions in smooth and stepped spillways are proposed.

2. Physical model

The physical model, tested by Ward in 2002, was located at Colorado State University (Ward, 2002). The concrete spillway was 34·09 m long, 1·22 m wide, and 2·13 m deep on a $2H$: $1V$ slope with a total height of 15·24 m. It is the same physical model as that used in the Hydraulic Laboratory Report HL-2005-06 which is one of the reports in the Hydraulic Laboratory Report series produced by the Bureau of Reclamation's Water Resources Research Laboratory in the United States (Frizell, 2006). There were three types of spillways with the schematic diagram and locations of measurement as shown in Figure 1(a).

(*a*) For the smooth spillway, flow discharges of 0·57, 1·13, 1·70, and 2·27 m^3/s were used. The data on the five locations were measured in the direction normal to the spillway floor. They were at $L_s/L = 0{\cdot}09$, 0·28, 0·44, 0·60, and 0·76, as shown in Figure 1(b).
(*b*) For the 25-step spillway, with $h = 0{\cdot}61$ m and $l = 1{\cdot}22$ m, values for y_c/h of 0·46, 0·73, 0·96, 1·16 and 1·48 were used and they are identified as $T_{0{\cdot}46}$, $T_{0{\cdot}73}$, $T_{0{\cdot}96}$, $T_{1{\cdot}16}$ and $T_{1{\cdot}48}$, respectively. The corresponding discharges are 0·57, 1·13,

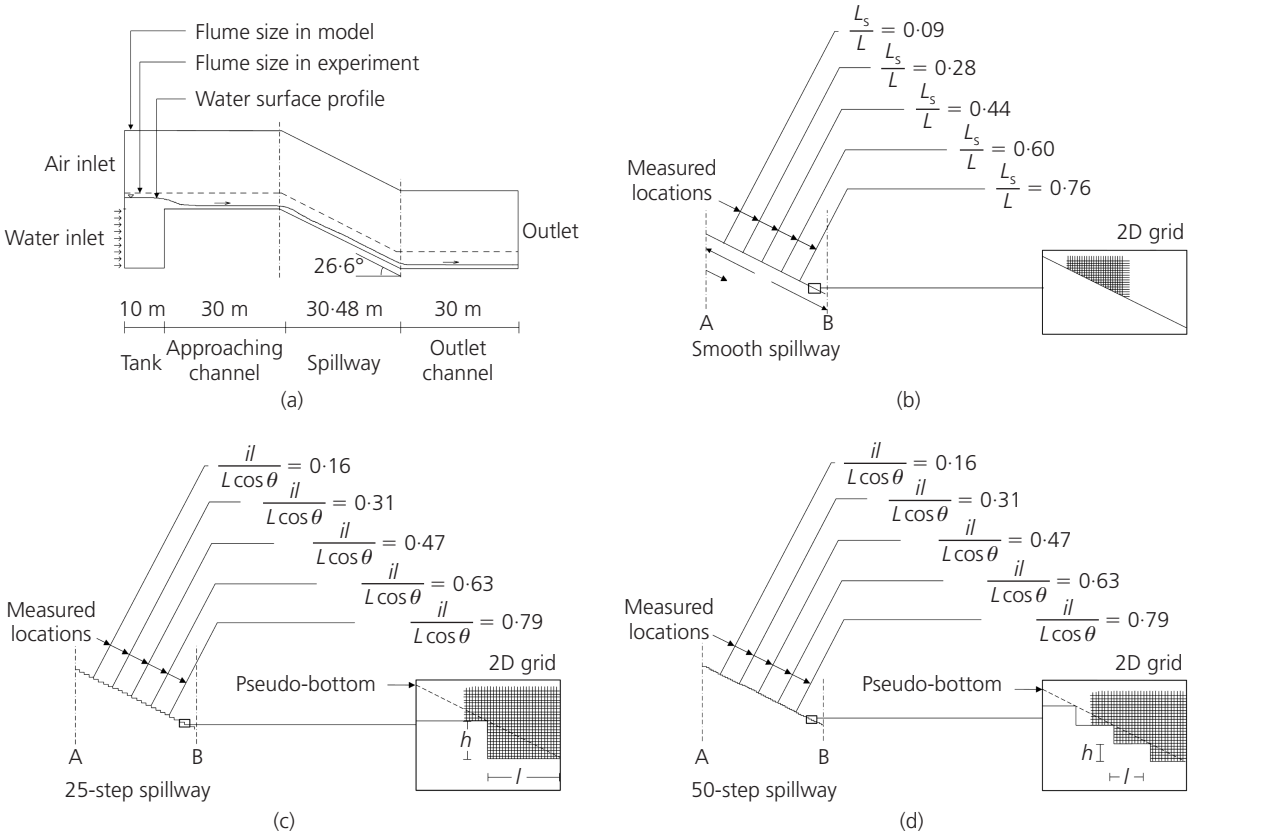

Figure 1. Schematic diagrams of spillways: (a) spillway dimension; (b) smooth spillway; (c) 25-step spillway, and (d) 50-step spillway

1·70, 2·27 and 3·28 m^3/s, respectively. The measurements were at the locations shown in Figure 1(c).

(*c*) For the 50-step spillway, with $h = 0{\cdot}31$ m and $l = 0{\cdot}61$ m, values for y_c/h of 0·96, 1·48, 1·91, 2·32 and 2·69 were used. These cases are identified as $F_{0{\cdot}96}$, $F_{1{\cdot}48}$, $F_{1{\cdot}91}$, $F_{2{\cdot}32}$ and $F_{2{\cdot}69}$, respectively. The corresponding discharges are 0·60, 1·16, 1·70, 2·27 and 2·83 m^3/s, respectively. The measurements were at the locations as shown in Figure 1(d).

Velocity and air concentration instrumentation was mounted on a carriage system. The manually operated carriage system allowed for two degrees of freedom, with movement along the spillway, and lateral movement within the width of the spillway. The remotely operated, motorised point gauge allowed for vertical movement normal to the pseudo-bottom. All profiles were taken along the centreline of the spillway. A back flushing Pitot-static tube was used to measure the velocity, due to its ability to work in non-homogeneous fluid. The output signal was scanned at 120 Hz for a duration of 20 s. The Pitot tube was patented by Leo *et al.* (1969) as a Strut mounted dual static tube No. US 3482445. The air probe was used to determine the air concentration. It acts as a bubble detector by passing a current through two conductors spaced approximately 2·0 mm apart and measures the change in conductivity that occurs when a bubble impinges on the probe tip. Its output signal was scanned at 15 kHz for 5 s per probe tip. The error on the vertical position of the probe was less than 0·025 mm. The accuracy on the longitudinal probe position was estimated as $\Delta x < \pm 0{\cdot}5$ cm.

3. Multiphase flow and turbulence models

3.1 Domain, mesh and set-up

The numerical model, commercial-Fluent, with the finite volume method (FVM) was used with the uniform-sized, structured grids. The meshed domain represents a two-dimensional (2D) grid as shown in Figure 1. The 2D grid was used because the results from the physical model were collected only at the centreline. Furthermore, the use of a 2D grid takes much less time than a three-dimensional (3D) grid.

The inlet section is upstream of the spillway which consists of the inlet of water at the bottom and the inlet of air at top. The inlet water velocity was the initial condition and was set uniformly at the water inlet and flow through the spillway which was initially full of air. The air boundaries were defined as an inlet pressure with the atmospheric pressure. The outlet of the

spillways at the downstream was defined as an outlet pressure such that the water could flow out freely. The simulation time in the model was 300 s, during which the flow had already become steady state in the physical model. The time for the computation for a typical case was about 60 h. The calculation domain was discretised into a structured grid with various sizes of $0{\cdot}035 \times 0{\cdot}035$, $0{\cdot}05 \times 0{\cdot}05$ and $0{\cdot}10 \times 0{\cdot}10\,\mathrm{m}^2$ quadrilateral cells.

The control volume technique was used to convert the governing equations to algebraic equations that could be solved numerically. The integration governing equations on the control volumes were solved iteratively using an implicit form. In the implicit scheme, the unknown value of each variable was computed from the relationship among the neighbouring meshes. Both known and unknown values from the neighbouring meshes werere used in one equation to evaluate the unknown value as [unknown = *function* (known + (unknown & known from neighbouring meshes))]. Therefore, each unknown value was used in more than one equation. These equations were solved simultaneously to get the values of the unknown quantities. The advantage of the implicit scheme is that it is unconditionally stable with respect to time step size.

The volume of fluid (VOF) model (Hirt and Nichols, 1981) was chosen as a multiphase model and the realisable k–ε model was chosen as turbulence.

3.2 The volume of fluid model

The VOF formulation, one of the Eulerian–Eulerian models, based on the concept that there can be more than two phases in each control volume and they are not interpenetrating (Hirt and Nichols, 1981). In the free surface flow, as in the present study, the interface between air and water is tracking. Therefore, it is appropriate to use the VOF model because the interface cell can be tracked as a mixture cell whereas the other Eulerian–Eulerian models focus only on the bubbles. The results from the Eulerian–Eulerian mixture model were previously found to be unsatisfactory by the authors, especially at the interface, and so it was not used in the present study. The properties in any cell are either purely representative of one of the phases or representative of a mixture. For a cell with a mixture, all properties are shared by the phases and represent volume-averaged values. Due to the concept of volume fraction, the properties, such as velocity, pressure and temperature, are shared. The total volume fractions of all phases in each domain cell sum to unity, the cell density can be calculated from

$$\rho = \alpha_{\mathrm{w}}\rho_{\mathrm{w}} + \alpha_{\mathrm{a}}\rho_{\mathrm{a}} = \alpha_{\mathrm{w}}\rho_{\mathrm{w}} + (1-\alpha_{\mathrm{w}})\rho_{\mathrm{a}} \quad (1)$$

The other variables can also be calculated by using the same fraction of Equation 1. The volume fraction of fluid can be: 0 if the cell contains no fluid of that kind; 1 if it is full of that fluid; and in between 0 and 1 if it is a mixture cell.

The VOF solves a set of continuity and momentum equations and tracks the volume fraction of each phase by a tracking equation, Equations 2, 3 and 4, respectively

$$\frac{\partial \rho}{\partial t} + \frac{\partial \rho u_i}{\partial x_i} = 0 \quad (2)$$

$$\frac{\partial \rho u_i}{\partial t} + \frac{\partial \rho u_i u_j}{\partial x_j} = -\frac{\partial P}{\partial x_i} + \frac{\partial}{\partial x_j}(\mu + \mu_{\mathrm{t}})\left(\frac{\partial u_i}{\partial x_j} + \frac{\partial u_j}{\partial x_i}\right) \quad (3)$$

$$\frac{\partial \alpha_{\mathrm{w}}}{\partial t} + u_i \frac{\partial \alpha_{\mathrm{w}}}{\partial x_i} = 0 \quad (4)$$

3.3 The realisable k–ε model

Because the steps act as a macro roughness, flow through the spillway is a highly turbulent, two-phase flow that can generate high rates of momentum transfer. Therefore, using the turbulence model is important to obtain good results for turbulent flow behaviour. The realisable k–ε model was first proposed as a k–ε eddy viscosity model for high Reynolds number turbulent flows (Shih *et al.*, 1995). A new equation for dissipation rate was therefore suggested based on the dynamic equation of fluctuation at large turbulent Reynolds numbers.

The modelled transport equations for turbulent kinetic energy and turbulent dissipation rate in the realisable k–ε model are

$$\frac{\partial}{\partial t}(\rho k) + \frac{\partial}{\partial x_j}(\rho k u_j) = \frac{\partial}{\partial x_j}\left[\left(\mu + \frac{\mu_{\mathrm{t}}}{\sigma_k}\right)\frac{\partial k}{\partial x_j}\right] + G_k + G_{\mathrm{b}} - \rho\varepsilon - Y_{\mathrm{M}} + S_k \quad (5)$$

$$\frac{\partial}{\partial t}(\rho \varepsilon) + \frac{\partial}{\partial x_j}(\rho \varepsilon u_j) = \frac{\partial}{\partial x_j}\left[\left(\mu + \frac{\mu_t}{\sigma_\varepsilon}\right)\frac{\partial \varepsilon}{\partial x_j}\right] + \rho C_1 S_\varepsilon - \rho C_2 \frac{\varepsilon^2}{k + \sqrt{\upsilon\varepsilon}} + C_{1\varepsilon}\frac{\varepsilon}{k} C_{3\varepsilon} G_b + S_\varepsilon \quad (6)$$

This turbulence model uses the same equation for k as the other k–ε models. However, more variables were suggested in the equation for ε instead of constants and it was developed for flow with high Reynolds number from the exact solution. The performance is improved for good results in recirculation flow. The other Reynolds-averaged Navier-Stokes (RANS) models for ex-

ample; the standard k–ε, the renormalisation group (RNG) k–ε, the standard k–ω, the shear stress transport k–ω models, have been found to perform satisfactorily when used in different kinds of flow simulation. The standard k–ε is for fully turbulent flow and the effects of molecular viscosity are negligible although it gives poor predictions for swirling and rotating flows. The RNG k–ε significantly improved the accuracy for rapid flows but still does not predict the spreading of a round jet correctly. The standard k–ω was developed to work with compressibility, and shear flow spreading whereas the shear stress transport k–ω was developed to blend the robust and accurate formulation in the near-wall region. However, these RANS models have been used and compared by the authors in previous studies. As unsatisfactory results were found these models were not used in the present study.

4. Results and discussion

4.1 Grid independence study

In order to assess the discretisation error, the GCI was used. The methodology consisted of five steps (Celik *et al.*, 2008; Roache, 1997). First, define the representative grid sizes, then select three different grid resolutions with a grid refinement ratio, r_{ij}, of higher than 1·3. Then, the apparent order, p, is calculated from the equations as

$$p = \frac{\left|\ln\left|\frac{f_{32}}{f_{21}}\right| + q(p)\right|}{\ln r_{21}}$$

$$q(p) = \ln\left(\frac{r_{21}^{p} - s}{r_{32}^{p} - s}\right)$$

$$s = \operatorname{sign}\left(\frac{f_{32}}{f_{21}}\right) \quad (7)$$

Subscripts 1, 2, and 3 mean the finest, fine, and coarse grids, or the grid sizes of 0·035 × 0·035, 0·05 × 0·05, and 0·10 × 0·10 m^2, respectively. The next step is a calculation of the extrapolated solution and the extrapolated relative error from

$$f_{\text{ext}}^{ij} = \frac{r_{ij}^{p} f_j - f_i}{r_{ij}^{p} - 1} \quad (8)$$

$$e_{\text{ext}}^{ij} = \left|\frac{f_{\text{ext}}^{ij} - f_j}{f_{\text{ext}}^{ij}}\right| \quad (9)$$

Finally, the calculation of approximate relative error and GCI are given by

$$e_{\text{a}}^{ij} = \left|\frac{f_i - f_j}{f_j}\right| \quad (10)$$

$$GCI_{ij} = f_{\text{s}} \frac{e_{\text{a}}^{ij}}{r_{ij}^{p} - 1} \quad (11)$$

The values of GCI_{21}, which is the refinement between finest and fine grids, were less than 4%. In comparison, the values of GCI_{32} were less than 11%. It can be seen that the simulation was dependent on grid size. The change of grid size showed a large effect for all cases of spillways.

For the 50-step spillway, the values of e_{a}^{32} ranged from 10 to 20% whereas e_{a}^{21} was less than 5%. In the present study, the fine grid is suggested to be an appropriate size because it showed noticeably better results than the coarse grid, whereas it showed only a small difference compared to the finest grid. The maximum percentage differences between the experimental data and the coarse, fine, and finest grids were 61, 26 and 19%, respectively. The time and resources required for the simulation from the fine grid were less than for the finest grid, but it showed similar results. However the results from the 'finest grid size' were used in the present study with 1 700 008 and 1 688 188 cells for the 25-step and 50-step spillways, respectively.

The extrapolated numerical solution, f_{ext}^{ij}, and the extrapolated relative error, e_{ext}^{ij}, can be used to show the extrapolated results. In the present study, f_{ext}^{32} for all cases were similar to f_{ext}^{21} and the extrapolated relative error, e_{ext}^{32} for all cases were also similar to e_{ext}^{21}. However, these extrapolated numerical solutions were not used in the study because the numerical results were intended to compare with the experimental data.

4.2 Flow along stepped spillways

Chinnarasri and Wongwises (2004) proposed the minimum critical flow depth required for the onset of skimming flow and the maximum critical flow depth for the nappe flow regime. The nappe flow regime is a succession of free-falling nappe and jet impacts from one step onto the next one when the nappe cavity is fully aerated (Chanson, 2002). For the cases of $T_{0\cdot46}$ and $T_{0\cdot73}$, nappe flow was observed. With the higher discharge, an air pocket was observed while the falling jet disappeared, then the flow became a transition flow. The skimming flow regime was observed after the higher discharge approach; in the present study, it was observed at $T_{0\cdot96}$. Then the air pocket disappeared and the flow recirculation was observed. The flow was turbulent along the spillway with the Reynolds number of $5{\cdot}56 \times 10^5 \leqslant \text{Re} \leqslant 3{\cdot}68 \times 10^6$, $1{\cdot}68 \times 10^6 \leqslant \text{Re} \leqslant 7{\cdot}21 \times 10^6$, and $1{\cdot}19 \times 10^6 \leqslant \text{Re} \leqslant 5{\cdot}55 \times 10^6$ for the smooth, 25-step, and 50-step spillways, respectively. All of the values of Re found in the

present study were greater than 10^5, which suggested that the viscous effects in the momentum exchange were minimised.

Similarly to the physical models, two cases of nappe flow were found on the 25-step spillway. The interface between the water surface and air can be seen in the numerical results. The numerical results for nappe flow looked similar to the physical model. The wavy water surface with the air pockets underneath could be seen on the steps. For the flow along the entire spillway, the value of V_{90} can be found from Figure 2. In the nappe flow zone, at low relative critical flow depth, y_c/ih, V_{90} stays constant since s is less than 0·2, where $s = il/L\cos\theta$. At high y_c/ih, V_{90} stays constant for $s > 0{\cdot}4$. In the nappe flow regime, it can be obtained that the location where V_{90} stays constant depends directly on the relative critical flow depth.

In cases of the same inlet velocity, for example: $T_{0{\cdot}96}$ and $F_{1{\cdot}91}$, $T_{1{\cdot}16}$ and $F_{2{\cdot}32}$, the value of V_{90} from the 50-step spillway was smaller than from the 25-step spillway at the same location. This shows that at the same y_c/ih, the velocity, V_{90}, can rapidly vary for different locations. However, V_{90} can be constant after steps at $s > 0{\cdot}8$. It can be observed that low y_c/ih can produce constant V_{90} faster than high y_c/ih. The flow profile of low y_c/ih and high y_c/ih were therefore compared to locate the point of interest.

The behaviour of skimming flow could be divided into two zones: non-aerated and aerated. In the non-aerated zone, irrotational flow without air entrainment was observed. The water surface was quite smooth. After flow through some steps, the aerated zone was found where the free surface was wavy with full air entrainment. The separation point of the non-aerated and aerated zone is called the inception point. Downstream of the inception point can be divided into two further zones, namely gradually varied flow and uniform flow. In gradually varied flow, flow depth and other properties such as velocity and pressure, changed gradually. At the end point of the gradually varied flow, the attainment of uniform flow was observed.

4.3 Flow on the step

The step which was far away from the inception point and reached a uniform condition was used for observation. The nappe and skimming flow on the steps are shown in Figure 3(a) and (b), respectively. The photos taken from the experiments (Frizell, 2006) with the simulation results of flow direction and volume fraction of water are shown on the same scale. For nappe flow, the flow depth was low and the air pocket was found near the corner of the tread and riser. The numerical results show good agreement with the photograph, as shown in Figure 3(a). In the air pocket, there were small velocity vectors in different directions which meant that some water spilled in and out of the air pocket. Due to the complexity in this zone, it was difficult to measure the velocity or pressure, so there is an advantage to using the numerical model. However, it should be verified that the numerical model can satisfactorily simulate this kind of flow. The numerical results of the air concentration at the surface or at 90% air concentration also agreed well with the experimental data.

For skimming flow, flow recirculation was observed in the lower region. The air bubbles in the flow recirculation were distributed within the upper region. High air entrainment was found at the centre of the recirculation flow while the least flow velocity was found there. In the lower region, flow recirculation played an important role in governing the pressure. The negative gauge pressure could be found in the flow recirculation whereas the higher pressure could be found in the downstream half of the tread. With the same velocity inlet, the negative pressure in the stepped spillway was less than in the smooth spillway whereas the negative pressure in the smooth spillway could be found along

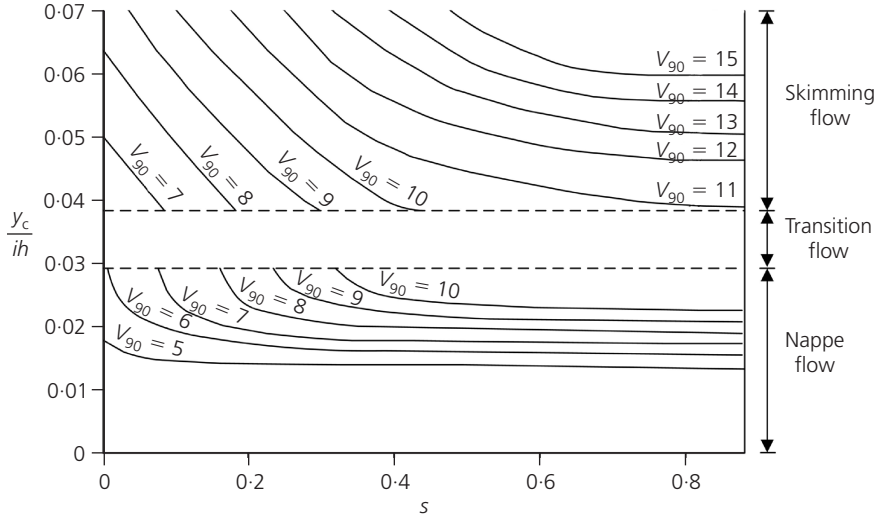

Figure 2. Diagram for V_{90} (m/s) at different dimensionless locations

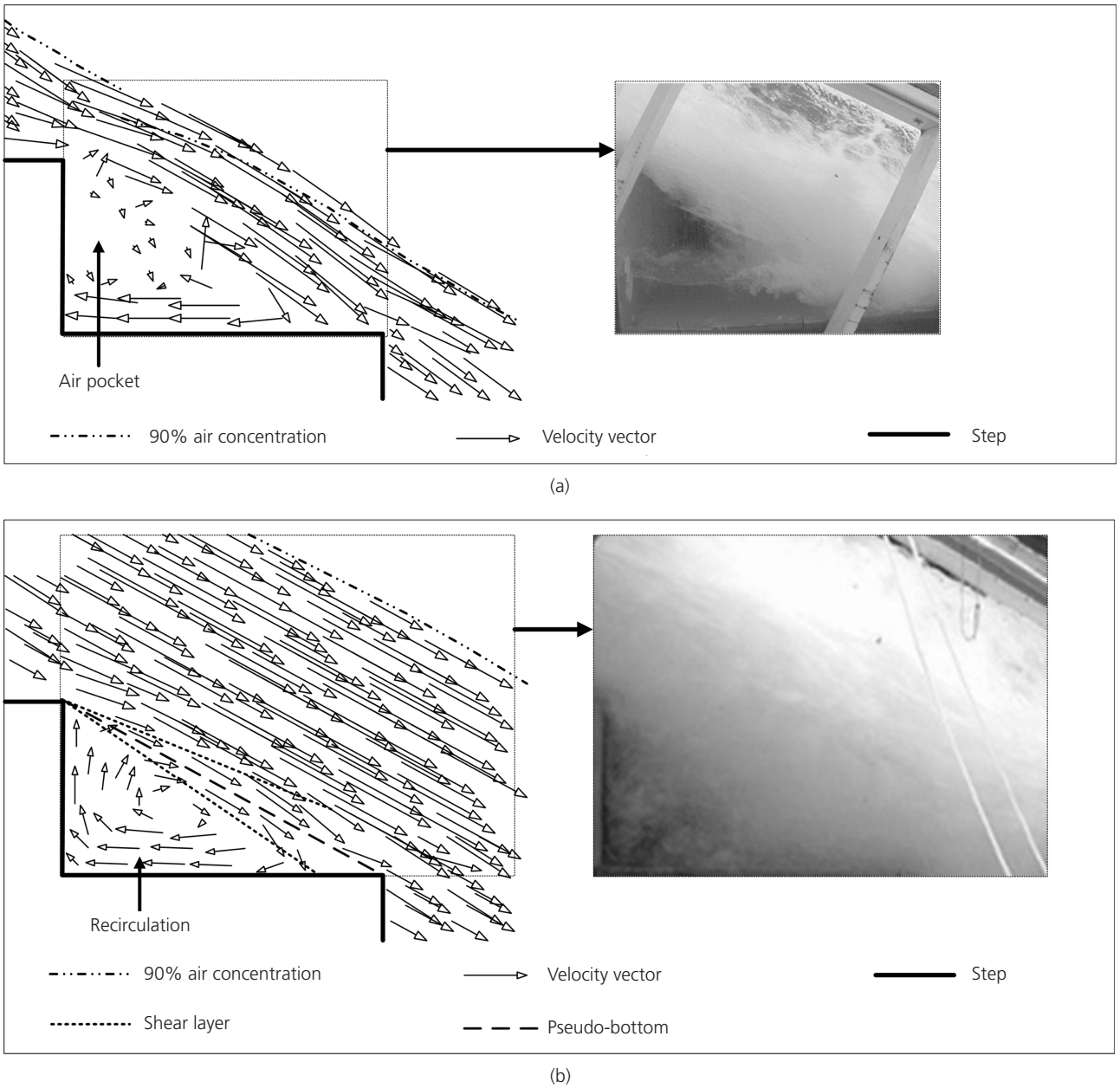

Figure 3. Schematic diagrams of flow on the steps (flow from left to right): (a) nappe flow; (b) skimming flow

the entire length wherever the flow depth was higher than the design head at the upstream. Therefore, prevention of damage from cavitation in a stepped spillway was easier than in a smooth spillway. The filling of more air into the recirculation can be one of the solutions to reduce the negative pressure. The numerical model can be a tool to design the appropriate step size for the reduction of the negative pressure.

The upper region, as shown in Figure 3(b), is the aerated zone. The flow depth in the main flow was higher than the nappe flow and contained a wavy water surface. The numerical results of the air entrainment near the surface agreed well with the experimental data but they could not simulate the region near the pseudo-bottom well. The interaction between lower and upper regions was characterised by a shear layer in the shear layer zone, as shown in Figure 3(b).

4.4 Velocity profile

The velocity profiles tended to have the same shape, beginning with velocity gradually increasing from the bed until a maximum velocity was reached. At some point in the upper region of the depth, an immediate change was observed where the velocity

abruptly increased. For both smooth and stepped spillways, the numerical results showed good agreement of the velocity profiles when compared with the experimental data. The velocity profiles along the smooth spillway at five stations with a discharge of 2·27 m^3/s are shown in Figure 4. The percentage difference between numerical and experimental data was less than 17%.

After flow along some distances through the spillway, the velocity profiles at all stations tended to have the same shape with the same maximum velocity. The maximum velocity at the last station near the outlet in the smooth spillway was high, and could cause more turbulence, compared with the flow along the stepped spillway at the same inlet velocity.

On the 25-step spillway, velocity profiles at $s = 0{\cdot}79$ between the physical and numerical models is shown in Figure 5. This location was chosen because it was far from both the inception point and the effect of tail-water. The percentage difference between the numerical and experimental data was less than 15%. It was found that near the water surface, the data from the physical model was quite different from the velocity profiles trend. This was due to a problem with measurements near the water surface with high turbulence of water and air. In the cases which had the same critical depth at the same location, the maximum velocity from the smooth spillway was higher than in the 25-step spillway. Thus, the stepped spillway was more efficient than the smooth spillway in reducing the flow velocity.

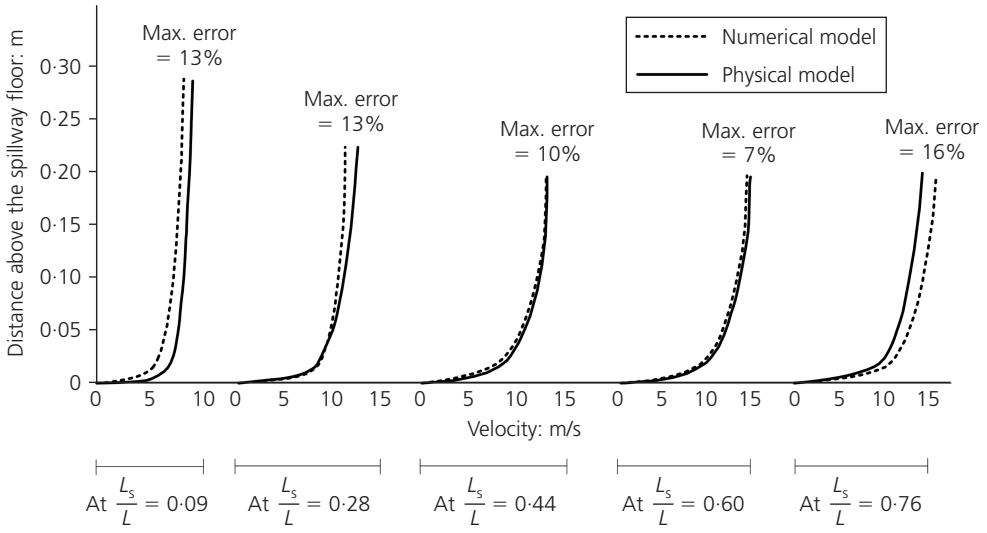

Figure 4. Velocity profiles at five locations along the smooth spillway with the discharge of 2·27 m^3/s

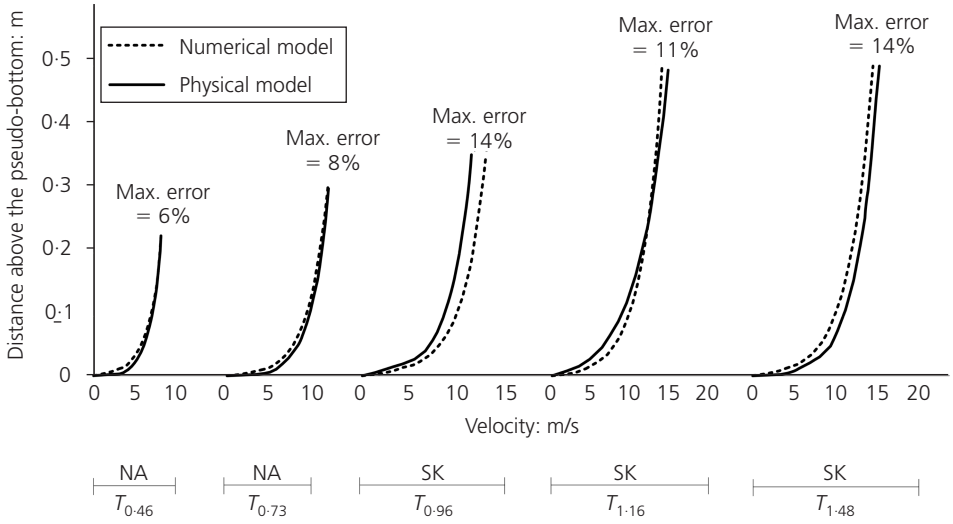

Figure 5. Velocity profiles on $il/L\cos\theta = 0{\cdot}79$ of 25-step spillway

For the 50-step spillway, the comparison of velocity profiles at $s = 0{\cdot}79$ in all cases is shown in Figure 6. The percentage difference between the numerical and experimental data was less than 12%. In a comparison of cases which had the same critical depth at the same location, the maximum velocity from the 25-step spillway was also higher than that for the 50-step spillway. Considering nappe flow only, Figure 7 shows the dimensionless velocity distribution at all five stations. In previous studies on skimming flow, the results followed the power law, as shown in Equation 12, suggesting different values of n.

$$\frac{V}{V_{90}} = \left(\frac{y}{y_{90}}\right)^{1/n} \quad 12.$$

Chanson and Toombes (2001) found $n = 5{\cdot}1$ and 6 for y_c/h values of 1·5 and 1·1, respectively. Matos (2000) obtained $n = 4$, whereas Chanson (1995) suggested $n = 3{\cdot}5$ and 4 for the earlier studies. However, in the present study, a value for n of 5 is then suggested at all five locations.

Concerning the skimming flow, the numerical results are shown in Figure 8. The power law of skimming flow for both the 25-step and 50-step spillways shows the same trend for all five locations. A value of $n = 4{\cdot}4$ was obtained from the present study, which was quite close to previous studies (Matos, 2000).

4.5 Turbulence intensity

The turbulence intensity in the flow through the spillway is subject to the influence of flow patterns of the boundary layers and boundary conditions of different sections. This can be defined as the ratio of root mean square of the longitudinal component of turbulent velocity over velocity at that point. In Figure 9, the turbulence intensity distributions from the smooth spillway, with an inlet discharge of 2·27 m^3/s, are shown with the flow direction from left to right. The trends of the turbulence intensity profiles were similar to those on the smooth open-channel flow in a previous study (Radhakrishnan and Piomelli, 2008).

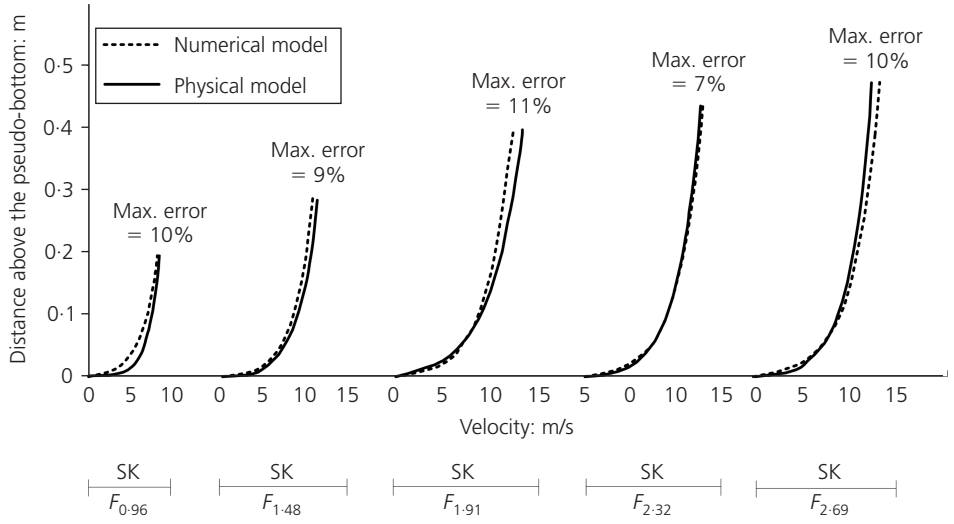

Figure 6. Velocity profiles on $il/L\cos\theta = 0{\cdot}79$ of 50-step spillway

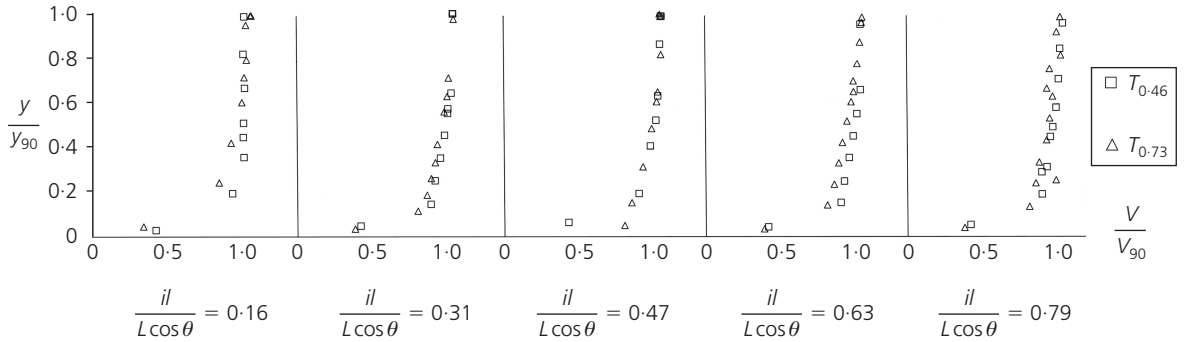

Figure 7. Dimensionless velocity distributions on different locations of nappe flow

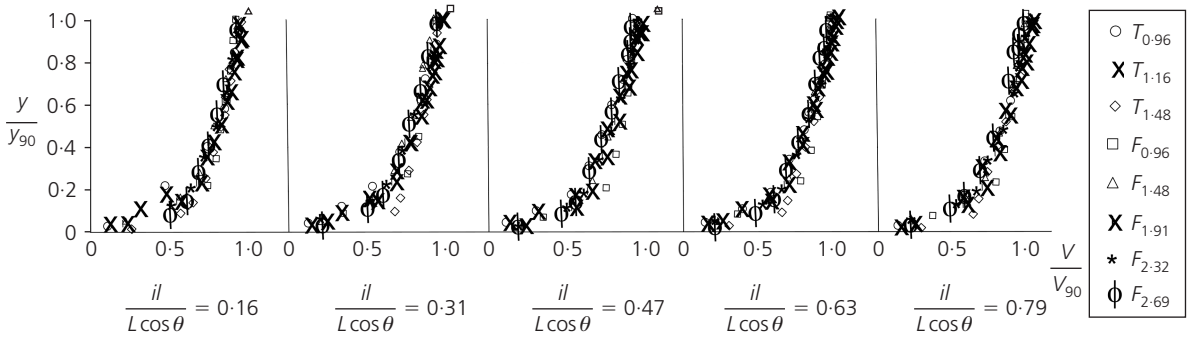

Figure 8. Dimensionless velocity distributions on different locations of skimming flow

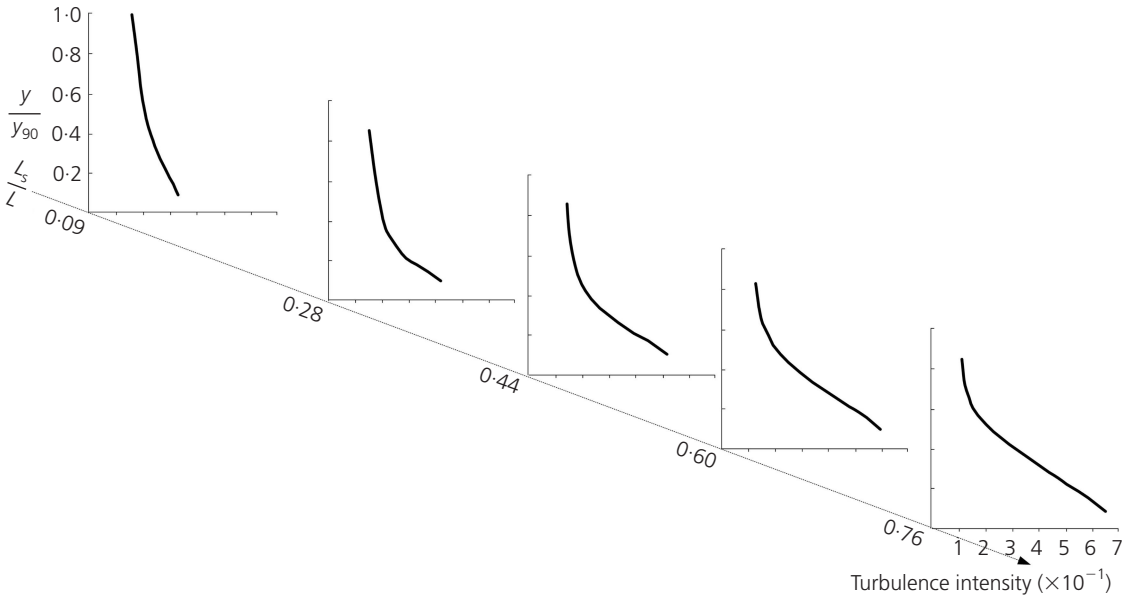

Figure 9. Turbulence intensity distributions of flow along smooth spillway with the inlet discharge of 2·27 m^3/s

At each measurement location, the maximum turbulence intensity, I_{max}, occurred close to the spillway floor. Then, with greater water depth, the turbulence intensity decreased to a minimum, I_{min}, near the water surface. For the location upstream, I_{max} is lower than at the stations downstream. It increased gradually along the spillway and reached a maximum near the outlet. With respect to I_{min} near the surface, it slowly decreased from upstream to downstream. On the other hand, it can be observed that both I_{max} and I_{min} for flow along the smooth spillway occur near the spillway outlet. From comparisons at the same location with a different critical depth, the flow with low critical depth obtained a value of I that was less than the high critical depth. Critical depth and flow distance have an obvious effect on turbulence intensity.

For the stepped spillway, the turbulence intensity in both nappe and skimming flow showed different trends from some previous studies (Chanson and Toombes, 2002; Gonzalez and Chanson, 2004). This might be because of the values of some of the parameters used to calculate the turbulence intensity. These previous studies used mean or average velocity to calculate the turbulence intensity. However, in comparison with the studies in which the turbulence intensity was from the friction velocity (Carollo *et al.*, 2005; Wang *et al.*, 1993), the results show the same trend. The equation for the distribution of turbulence intensity was used and it was shown as

$$\frac{u'}{u_*} = D\mathrm{e}^{-\lambda(y/H)} \quad (13)$$

The turbulence intensity distributions depend directly on the roughness ratio between the flow depth and roughness height. The

constants in Equation 13 can be divided into two groups based on H/K_s. However, in the present study, only H/K_s values of less than 0·4 were found. Therefore, the results were compared and it was found that all results were under values given by Equation 13 with $D = 2{\cdot}14$ and $\lambda = 0{\cdot}8$. The turbulence intensity distribution was found to decrease in the direction from the water surface to the pseudo-bottom. In the region where y/H took values of less than 0·2, the turbulence intensity was found to be quite constant with bed distance. It was also found that the roughness of the spillway considerably increased the turbulence intensity.

4.6 Energy dissipation

The energy dissipation, E_L/E_0, is one of the dimensionless parameters which is widely used. The energy loss, E_L, is the difference between energy at the inlet section, E_0, and the energy at the point-of-interest section, E_i. The point of interest is superimposed with the datum, then the energy E_i consists of flow depth measured in the vertical direction and the velocity head. The energy E_0 consists of the elevation of the head from the datum to the inlet, and the summation of flow depth and velocity head which is equal to $1{\cdot}5y_c$. The energy dissipation for the smooth spillway rapidly decreased with increasing discharge whereas for the stepped spillway it decreased only gradually. For a given height, the energy dissipation increased when the number of steps increased for the case of skimming flow. Because each step acts as a macro roughness, more steps caused more flow resistance and energy dissipation. With the results from the simulation, the empirical correlation for the energy dissipation on the critical depth and number of steps, with $R^2 = 0{\cdot}90$ and the limit of $2H$: $1V$ stepped spillway, is

$$\frac{E_L}{E_0} = 0{\cdot}94e^{-2{\cdot}84(y_c/ih)} \quad 14.$$

The results of Rad and Teimouri (2010), $0{\cdot}04 \leqslant y_c/ih \leqslant 0{\cdot}13$, fit very well with the results from the present study, which were $0{\cdot}02 \leqslant y_c/ih \leqslant 0{\cdot}60$. They were also compared with some other large-scale studies: Chanson and Toombes (2002) with a spillway slope of 15·9° and $3 \times 10^5 \leqslant Re \leqslant 8 \times 10^5$; Carosi and Chanson (2008) with a spillway slope of 21·8° and $3 \times 10^5 \leqslant Re \leqslant 7 \times 10^5$; and Chanson and Felder (2010) with a spillway slope of 26·6° and $5 \times 10^4 \leqslant Re \leqslant 1 \times 10^6$. The dimensionless residual head, E_i/y_c, is then used for comparison. For the slope of 21·8°, E_i/y_c was 3·1 and it was 4·6 for 15·9° and 26·6° depending on the step height. E_i/y_c was 4·5 from the present study, which is not much different from the previous investigation and confirmed the results from the other large-scale studies.

5. Conclusions

A numerical model was used to study the flow behaviour through smooth and stepped spillways. The stepped spillways consist of 25 and 50 steps. The numerical results were verified by comparison with the large-scale physical model. By using GCI, a grid size of $0{\cdot}05 \times 0{\cdot}05\ m^2$ was an appropriate grid size because it showed a small difference of less than 5% when compared with the grid size of $0{\cdot}035 \times 0{\cdot}035\ m^2$. It also showed a small percentage difference compared with the experimental data. The flow and velocity profiles from the numerical model showed good agreement with the experimental data. By using the numerical results, the diagram for flow velocity at 90% air concentration at different dimensionless locations is proposed. From this diagram, the location of uniform flow in different critical flow depths can be found. The constants in the equations for the power law of the velocity profile (Equation 12) and the distribution of turbulence intensity (Equation 13) were proposed. An empirical correlation for energy dissipation of flow through stepped spillways is suggested (Equation 14).

Acknowledgements

The authors would like to thank the Thailand Research Fund/ Royal Golden Jubilee PhD Grant (PHD/0225/2548 and BRG5280001) for financial support. Partial support from the National Research University Project of Thailand's Office of the Higher Education Commission is greatly appreciated. Sincere thanks to Professor James F. Ruff, and Professor Robert N. Meroney from Colorado State University for their supporting data, facilities and recommendations.

REFERENCES

Boes R and Hager WH (2003) Two-phase characteristics of stepped spillways. *Journal of Hydraulic Engineering* **129(9)**: 661–670.

Carollo FG, Ferro V and Termini D (2005) Analyzing turbulence intensity in gravel bed channels. *Journal of Hydraulic Engineering* **131(12)**: 1050–1061.

Carosi G and Chanson H (2008) Turbulence characteristics in skimming flows on stepped spillways. *Canadian Journal of Civil Engineering* **35(9)**: 865–880.

Celik IB, Ghia U, Roache PJ *et al.* (2008) Procedure for estimation and reporting of uncertainty due to discretization in CFD applications. *Journal of Fluid Engineering* **130(7)**: 1–4.

Chamani MR and Rajaratnam A (1999) Characteristics of skimming flow over stepped spillways. *Journal of Hydraulic Engineering* **125(4)**: 361–368.

Chanson H (1995) *Hydraulic Design of Stepped Cascades, Channels, Weirs and Spillways*. Pergamon, Oxford, UK.

Chanson H (2002) *The Hydraulics of Stepped Chutes and Spillways*. Balkema, Lisse, the Netherlands.

Chanson H and Felder S (2010) Energy dissipation on embankment dam stepped spillways, overflow stepped weirs and masonry stepped spillways. In *Proceedings of the 17th Congress of IAHR Asia and Pacific Division, Auckland, New Zealand* (Melville B, Costa GD and Swann T (eds)).

Chanson H and Toombes L (2001) *Experimental Investigations of Air Entrainment in Transition and Skimming Flows Down a Stepped Chute: Application to Embankment Overflow Stepped Spillways*. Department of Civil Engineering, University of Queensland, Australia.

Chanson H and Toombes L (2002) Air-water flows down stepped

chutes: Turbulence and flow structure observations. *International Journal of Multiphase Flow* **28(11)**: 1737–1761.

Chen Q, Dai GQ and Liu HW (2002) Volume of fluid model for turbulence numerical simulation of stepped spillway overflow. *Journal of Hydraulic Engineering* **128(7)**: 683–688.

Cheng XJ, Chen YC and Luo L (2006) Numerical simulation of air-water two-phase flow over stepped spillways. *Science in China Series E: Technological Sciences* **49(6)**: 674–684.

Chinnarasri C and Wongwises S (2004) Flow regimes and energy loss on chutes with upward inclined steps. *Canadian Journal of Civil Engineering* **31(5)**: 870–879.

Frizell KH (2006) *Research State-of-the-art and Needs for Hydraulic Design of Stepped Spillways*. US Department of the Interior Bureau of Reclamation, Denver, Colorado, Report HL-2005-06.

Gonzalez AC and Chanson H (2004) Scale effects in moderate slope stepped spillways experimental studies in air-water flows. In *The 8th National Conference on Hydraulics in Water Engineering, Gold Coast, Australia*.

Hirt CW and Nichols BD (1981) Volume of fluid (VOF) method for the dynamics of free boundaries. *Journal of Computational Physics* **39(1)**: 201–225.

Matos J (2000) Hydraulic design of stepped spillways over RCC dams. In *Proceedings of the International Workshop on Hydraulics of Stepped Spillways* (Minor HE and Hager WW (eds)). Balkema, Lisse, the Netherlands, pp. 187–194.

Rad IN and Teimouri M (2010) An investigation of flow energy dissipation in simple stepped spillways by numerical model. *European Journal of Scientific Research* **47(4)**: 544–553.

Radhakrishnan S and Piomelli U (2008) Large-eddy simulation of oscillating boundary layers: Model comparison and validation. *Journal of Geophysical Research* **113(2)**: 1–14.

Leo RVD, Hagen HW and Hagen FW (1969) *Strut Mounted Dual Static Tube*. Patent No. US 3482445. United States Patent Office Ser. No. 724176.

Roache PJ (1997) Quantification of uncertainty in computational fluid dynamics. *Annual Review of Fluid Mechanics* **29(1)**: 123–160.

Shih TH, Liou WW, Shabbir A, Yang Z and Zhu J (1995) A new k–ε eddy viscosity model for high Reynolds number turbulent flows. *Computers and Fluids* **24(3)**: 227–238.

Wang J, Dong Z, Chen C and Xia Z (1993) The effects of bed roughness on the distribution of turbulent intensities in open channel flow. *Journal of Hydraulic Research* **31(1)**: 89–98.

Ward JP (2002) *Hydraulic Design of Stepped Spillways*. PhD dissertation, Colorado State University, Colorado, USA.